IEEE Photonics Journal
An IEEE Photonics Society Publication

Ultracompact Electroabsorption Modulators Based on Tunable Epsilon-Near-Zero-Slot Waveguides

Volume 4, Number 3, June 2012

Zhaolin Lu
Wangshi Zhao
Kaifeng Shi

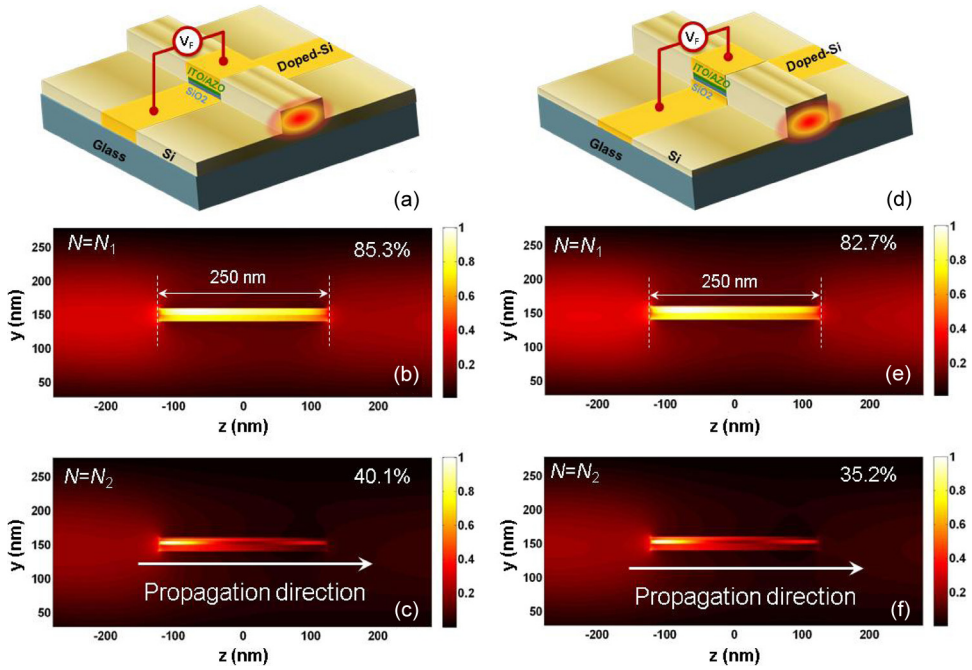

DOI: 10.1109/JPHOT.2012.2197742
1943-0655/$31.00 ©2012 IEEE

Ultracompact Electroabsorption Modulators Based on Tunable Epsilon-Near-Zero-Slot Waveguides

Zhaolin Lu, Wangshi Zhao, and Kaifeng Shi

Microsystems Engineering, Kate Gleason College of Engineering, Rochester Institute of Technology, Rochester, NY 14623-5603 USA

DOI: 10.1109/JPHOT.2012.2197742
1943-0655/$31.00 ©2012 IEEE

Manuscript received April 3, 2012; revised April 25, 2012; accepted April 26, 2012. Date of publication May 5, 2012; date of current version May 8, 2012. This material is based upon work supported in part by the U.S. Army under Award No. W911NF-10-1-0153 and the National Science Foundation under Award No. ECCS-1057381. Corresponding author: Z. Lu (e-mail: zhaolin.lu@rit.edu).

Abstract: We present a promising application of epsilon-near-zero (ENZ) materials in optical modulators. When a thin ENZ film is sandwiched in a single-mode waveguide, an ENZ-slot waveguide is formed, where the absorption can be greatly enhanced. We propose electroabsorption modulators based on tunable ENZ materials and slot waveguides. Transparent conducting oxides (TCOs) may be employed as the active slot, which can be tuned between ENZ (high absorption) and epsilon-far-from-zero (low absorption) by accumulation carriers. Numerical simulation shows that over 3-dB modulation depth can be achieved in a 250-nm-long TCO-slot waveguide. The modulators have the advantages of nanoscale footprints, small insertion loss, potentially ultrahigh speed, and easy fabrication.

Index Terms: Metamaterials, optoelectronic materials, silicon nanophotonics.

1. Introduction

The development of metamaterials has opened new horizons in photonics [1], [2]. Recent research shows that the dielectric constant of materials can be engineered to be almost any arbitrary value (positive, zero, or negative). One example is epsilon-near-zero (ENZ) materials [3]–[5], which have received significant attention and found applications in squeezing electromagnetic energy through very narrow channels [6], [7], design of matched zero-index materials [5], [8], as well as shaping the radiation pattern of a source [3], [9]. Recently, we found that light absorption can be greatly enhanced in ENZ-slot waveguides even when the slot thickness is less than 1 nm [10]. In that case, graphene works as a tunable ENZ material for telecom wavelengths. We showed that up to 3-dB modulation depth can be achieved within 800 nm long Si waveguides, or 120 nm long plasmonic waveguides. The result is very promising, but the fabrication of graphene-sandwiched waveguides may be a challenge. More recently, more ENZ materials were discovered, for example, transparent conducting oxides (TCOs), which are compatible with semiconductor processes, tunable in optical properties, and with low intrinsic loss. Based on TCOs, even more compact modulators may be achieved. Herein, we present our exploration on electroabsorption (EA) modulators based on TCO-slot waveguides.

The effect of free carriers on an optical material can be approximated by the Drude model, $\varepsilon = \varepsilon_\infty - \omega_p^2/\omega(\omega + j\gamma)$. Here, ε_∞ is the high frequency dielectric constant, γ is the electron damping factor, ω is the angular frequency of the light wave, and ω_p is the plasma frequency given by $\omega_p^2 = Ne^2/\varepsilon_0 m^*$, which depends on carrier concentration N, and the effective electron mass m^*. As

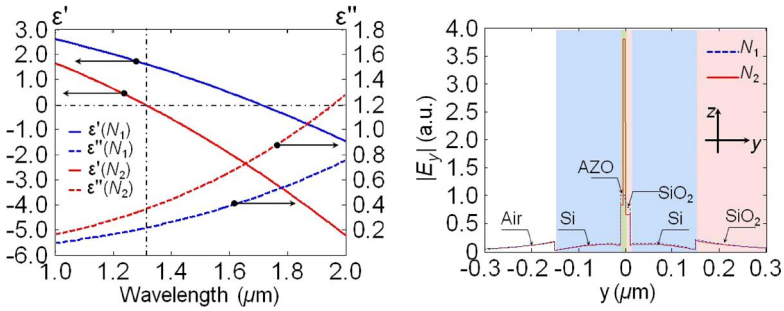

Fig. 1. (a) Real part and imaginary part of the dielectric constant of AZO as a function of wavelength at two different carrier concentrations based on the Drude model. (b) The plots of the transverse electric field magnitude across the waveguide at $N = N_1$ and $N = N_2$, respectively.

a result, the ENZ effect can be seen in many materials at $\omega \approx \omega_p/\sqrt{\varepsilon_\infty}$, for example tungsten at $\lambda_0 = 48.4$ nm with $\min\{|\varepsilon(\mathrm{W})|\} = 0.483$, and aluminum at $\lambda_0 = 83$ nm with $\min\{|\varepsilon(\mathrm{Al})|\} = 0.035$ [11]. However, the plasma frequencies of most metals are located in the UV regime due to their ultrahigh electron density. To make ENZ located in the near infrared (NIR) regime, the electron density should reduce to $10^{20} \sim 10^{21}/\mathrm{cm}^3$, which coincides that of TCOs. Recently, considerable effort has been focused on TCOs as the plasmonic and ENZ metamaterial for NIR applications [12]–[16]. Feigenbaum *et al.* [17] have studied the refractive index changes in the accumulation layer of a metal–oxide–TCO heterostructure, and experimentally showed that carrier concentration at the oxide/TCO interface can increase from 1×10^{21} /cm^3 to $1 \times 10^{22}/\mathrm{cm}^3$ under a few volts across a 100 nm thick oxide. In particular, the crossover wavelength, where real permittivity crosses zero, of indium tin oxide (ITO) shifts from 1918 nm to 1136 nm with only 1.0 V. Noginov *et al.* [18] and Naik *et al.* [19], [20] did comparative studies independently, and showed that aluminum-doped zinc oxide (AZO) has even smaller absorption than ITO in the NIR regime. Therefore, we choose AZO as an example material from various TCOs. Devices based on other TCOs may result in similar performance as we will describe below.

2. Tunable ENZ-Slot Waveguides

Based the measured dielectric constant reported in [18], we extracted $\varepsilon_\infty = 4.0$, $\omega_p = 2.22 \times 10^{15}$ s^{-1}, and $\gamma = 1.30 \times 10^{14}$ s^{-1} for AZO. The carrier concentration can be estimated as $N_1 = 4.19 \times 10^{20}$ cm^{-3} ($m^* = 0.27m_0$). The crossover wavelength is located at 1710 nm, and $\varepsilon_1 = 1.636 + \mathrm{j}0.214$ at $\lambda_0 = 1310$ nm, the operation wavelength of the EA modulator to be designed. With a suitable applied voltage, the carrier concentration can increase to $N_2 = 7.08 \times 10^{20}$ cm^{-3}, which is 1.69 times of N_1, and this value is practical according to recent work [17]. Based on the Drude model, the crossover wavelength shifts to 1310 nm with $\varepsilon_2 = 0.004 + \mathrm{j}0.361$. Fig. 1(a) shows the dielectric constant (real part and imaginary part) as a function of wavelength under N_1 and N_2. Note that the magnitude of the dielectric constant has changed $|\varepsilon_1|/|\varepsilon_2| = 4.57$ times. In this sense, AZO and other TCOs may be good EA materials. Indeed, TCOs have been proposed as the active media in several plasmonic modulators [21]–[23]. However, the ultrathin ($\sim$5 nm) accumulation layer and inherent absorption downplay their role in most optoelectronic devices. To this end, some novel waveguides and platforms need to be employed to enhance the interaction. In this paper, we apply the principle of our graphene-slot waveguides and propose EA modulators based on AZO-slot waveguides.

A slot waveguide [24] can be formed when a very thin low-index film (slot) is sandwiched inside a single-mode waveguide. In our case, we consider a 10-nm AZO film is sandwiched in a doped-Si waveguide with 10-nm SiO_2 buffer layer, as shown in Fig. 1(b). The slot waveguide works only for the transverse magnetic (TM) mode, where the magnetic field is parallel to the low-index thin film, i.e., $H = H_x$ in Fig. 1(b) (x-axis, not shown in the figure to avoid confusing, is perpendicular to the yoz plane). Due to the continuity of normal electric flux density, the dominate electric field

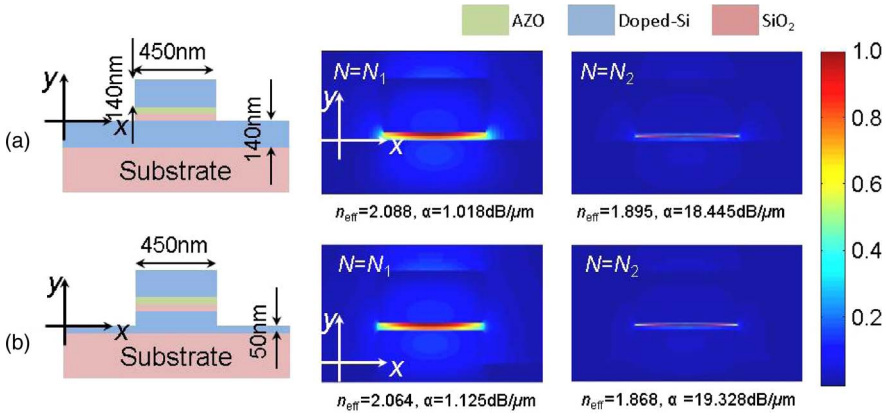

Fig. 2. Electric field profiles, effective indices, and propagation loss for different AZO-slot waveguides at $N = N_1$ and $N = N_2$, respectively: (a) in a slot rib waveguide; (b) in an over etched slot rib waveguide. The maximum field magnitude is normalized to be 1 in each plot. The refractive indices of Si, and SiO_2 are assumed to be 3.47 and 1.45, respectively. Both the thickness of the AZO and buffer layers are 10 nm.

component is inversely proportional to the slot dielectric constant, or $\varepsilon_1 E_{1y} = \varepsilon_2 E_{2y}$, where the free charge effect is included in the complex dielectric constant. Note E_y is the dominate component of the electric field for the TM polarization. As a result, ENZ-slot can greatly enhance the electric field in the slot, and a large portion of guided power can be confined in the slot. An extreme case is a Dirac-function mode profile with 100% of power confined in the slot when the dielectric constant and thickness of the slot simultaneously approach to zero.

However, an ENZ material always comes with absorption. Without loss of generality, we assume its dielectric constant to be $\varepsilon = \varepsilon' + j\varepsilon'' = \varepsilon' + j\sigma/\omega\varepsilon_0$ for monochromatic light $(e^{-j\omega t})$, where σ is the conductivity of the material at the optical frequency. The power absorbed by the ENZ material in a unit volume

$$p_d = \frac{1}{2}\sigma E^2 \propto \frac{1}{2}\varepsilon'' E^2 \propto \frac{1}{2}\varepsilon''/|\varepsilon|^2$$

can be greatly enhanced at ENZ because (1) $|E_y|$ reaches its maximum and (2) $\varepsilon''/|\varepsilon|$ nearly grows to its maximum at the same time. To maximize the absorption, the magnitude of dielectric constant of the slot should decrease to zero as close as possible. Note the above equation is valid for infinitesimal slot thickness. Otherwise, the guided power will redistribute, and the operation of the slot waveguide fails if the slot thickness is too large.

To verify the enhancement, we solved the mode of the 2-D AZO-slot waveguide shown in Fig. 1(b) based on the transfer matrix method. Both the top and bottom doped-Si layers are chosen to be 140 nm thick. We assume the carrier concentration increases from N_1 to N_2 within 5 nm (accumulation layer thickness) over the oxide buffer layer when a suitable voltage is applied. On the other hand, the rest AZO beyond the accumulation layer is assumed not affected by the voltage. As shown in Fig. 1(b), the electric field can be greatly enhanced in the accumulation layer at $\lambda_0 = 1310$ nm when accumulation layer carrier concentration increases from N_1 to N_2. In particular, the magnitude of E_y boosts about 3.8 times, which is smaller than $|\varepsilon_1|/|\varepsilon_2|$ because the thickness of the slot is not infinitesimal.

3. Nanoscale EA Modulators

Based on the sandwiched structure, we use a 3-D mode solver to determine the optimal waveguide width based on the finite-difference time-domain (FDTD) method. Considering the fabrication tolerance, the optimal width of the waveguide is found to be 450 nm. Fig. 2(a) shows the mode profiles of the AZO-slot waveguide at different carrier concentrations. There is a considerable shift

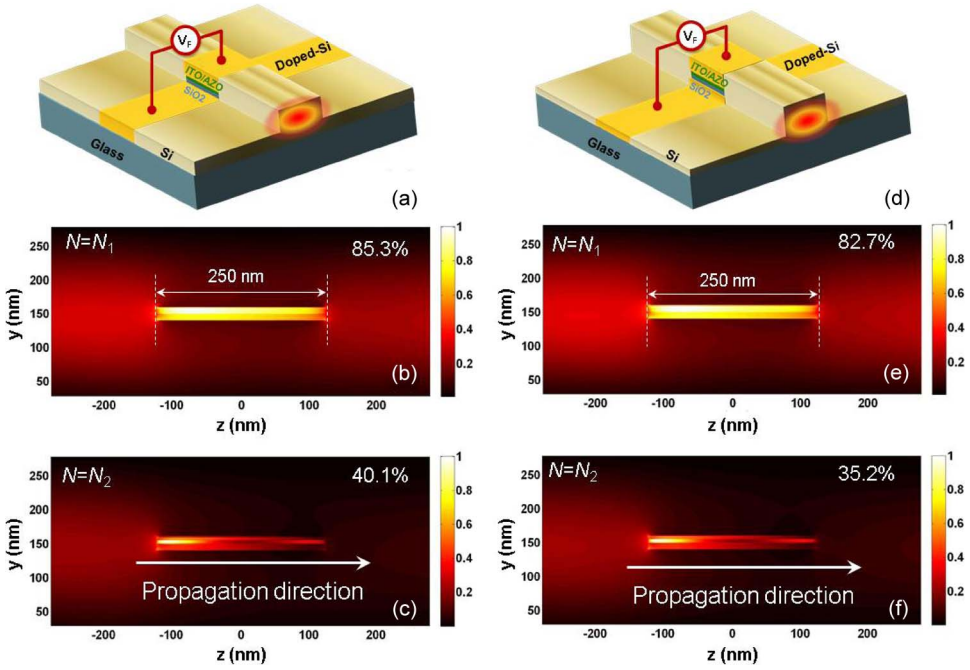

Fig. 3. (a) The illustration of an EA modulator embedded on a rib Si waveguide. The cross section dimensions of the modulator are shown as Fig. 2(a). (b), (c) The 3-D simulation of light propagation between a rib Si waveguide and the EA modulator at $N = N_1$ and $N = N_2$, respectively. (d) The illustration of an EA modulator embedded on an over etched rib Si waveguide. The cross section dimensions of the modulator are shown as Fig. 2(b). (e), (f) The 3-D simulation of light propagation between an over etched rib Si waveguide and the EA modulator at $N = N_1$ and $N = N_2$, respectively.

in the effective index: 2.09 at $N = N_1$, and 1.90 at $N = N_2$. Thus, quite compact phase modulators based on Mach–Zehnder interferometer or microring may be achieved. More importantly, there is a huge change in the waveguide attenuation. At $N = N_1$, the $|E_y|$ in the accumulation layer is slightly higher than in the SiO_2 buffer layers, and the waveguide works at the low loss state with $\alpha_1 = 1.0$ dB/μm; at $N = N_2$, the $|E_y|$ in the accumulation layer is many times higher than in the SiO_2 buffer layers, and the waveguide works at the high absorption state with $\alpha_2 = 18.4$ dB/μm. As a result, modulation depth 17.4 dB/μm can be achieved, and 3 dB-modulation depth only requires 173 nm propagation distance! A 250-nm propagation distance results modulation depth 4.36 dB. A more confined mode may be achieved by over etching the bottom Si layer of the waveguide as shown in Fig. 2(b). Simulation shows a slight improvement in the performance. In particular, the modulation depth increases to 18.2 dB/μm.

To evaluate the insertion loss of the EA modulators, we performed 3-D FDTD simulations with the smallest mesh size down to 0.5 nm. In the simulations, we assume the modulators are embedded in Si waveguides with same overall dimensions as themselves except without the AZO and buffer layers. We first simulated the modulator based on the rib waveguide platform as shown in Fig. 3(a). The length of the EA modulator is 250 nm. Fig. 3(b) and (c) show the power distribution in the waveguide at $N = N_1$ and $N = N_2$, respectively. Simulation results demonstrate that the overall throughput is 85.3% at $N = N_1$, and 40.1% at $N = N_2$. Note that the insertion loss is only 0.69 dB (85.3%). The achievable modulation depth, 3.3 dB, is smaller than the one predicted by the 3-D mode solver. This is due to the mode mismatch between the slot waveguide of the modulator and its input/output rib waveguide. Replacing the rib waveguides with slot waveguides may further reduce the insertion loss. For the over etched rib waveguide structure illustrated in Fig. 2(b), similar performance can be achieved as shown in Fig. 2(d)–(f). With the same 250 nm propagation length, the throughput is 82.7% at $N = N_1$, and 35.2% at $N = N_2$, respectively. The calculated insertion loss is 0.82 dB and the modulation depth is 3.7 dB.

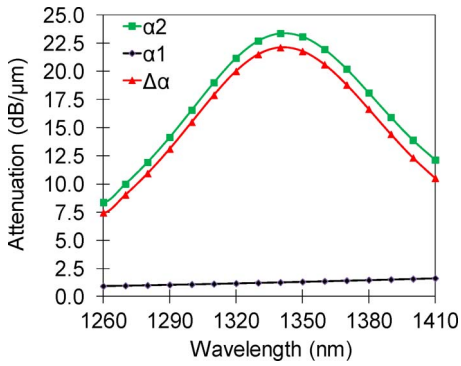

Fig. 4. Attenuation of AZO-slot waveguide as a function of working wavelength at N_1 and N_2, respectively. All data are for the TM mode of the slot waveguide illustrated in Fig. 2(a).

The design of the EA modulator is ultracompact and has much lower insertion loss compared with previous works, in which a modulation depth around 3 dB need the modulator lengths of 4 μm [25] and 50 μm [26], respectively. In most works, the insertion loss is either not reported or quite large. For example, the insertion loss is over 3.7 dB in [26].

4. Performance Analysis

High-speed optical interconnects require a broad bandwidth. Based on the Drude model, we studied the bandwidth of the EA modulator by solving the modes shown in Fig. 2(a) at different working wavelengths. Fig. 4 shows the waveguide absorption as a function of wavelength in a Si waveguide. As can be seen, the attenuation of the modulator at $N = N_1$ nearly remains a constant, 0.92–1.63 dB/μm, while the attenuation at $N = N_2$ tops at 1340 nm. Again, the shift of the optimal working wavelength may be attributed to the non-infinitesimal thickness of the slot. In particular, the attenuations are 19.0 dB/μm, 23.4 dB/μm, and 20.2 dB/μm at 1310 nm, 1340 nm, and 1370 nm, respectively. Wavelength spanning from 1310 nm to 1370 nm, or 10 THz bandwidth, only decreases modulation depth 4.4 dB/μm.

The EA modulators can potentially work at an ultrahigh speed, being mainly limited by the RC delay imposed by electric circuits. The resistance (R) and capacitance (C) of the modulator mainly come from the doped silicon waveguide and the buffer layer, respectively. Assume the carrier concentration in the n-doped silicon is 1×10^{18} cm^{-3} and the corresponding resistivity can be calculated as $\rho_{Si} = 0.0225\ \Omega \cdot$ cm. We can estimate $RA = \rho_{Si} t_{Si} = 3.15 \times 10^{-11}\ \Omega \cdot \text{m}^2$, where A is the footprint of the modulator, and $t_{Si} = 140$ nm is the thickness of the top silicon layer. The capacitance can be estimated according to the accumulation charge and applied voltage: $C = \Delta Q/\Delta V$ and $C/A = \Delta N_s e/\Delta V = (N_2 - N_1) d_{Ac} e/\Delta V = 0.231$ F/m^2, which may be overestimated by assuming $\Delta V = 1.0$ V. $d_{\text{Ac}} = 5$ nm is the accumulation layer thickness. As a result, $RC \approx 7.28$ ps. The speed of the modulator will be investigated in our experimental work.

The proposed modulators can be potentially fabricated with a series of standard semiconductor processes. AZO will be fabricated using the pulsed-laser deposition. The buffer layer will be either SiO_2, or high-k materials (e.g., Al_2O_3 or HfO_2), which can be fabricated by oxidation or atomic layer deposition.

5. Conclusion

To summarize, we investigated the unique performance of the slot waveguide and found that light absorption can be greatly enhanced in an ENZ-slot waveguide. By combing recent progress on TCOs, we proposed and modeled EA modulators based on tunable ENZ-slot waveguides. These EA modulators promise to remove the technical bottleneck in on-chip optical interconnects with the advantages of nanoscale footprints, small insertion loss, potential ultrahigh speed, and easy fabrication.

Acknowledgment

Acknowledgment is made to the Donors of the American Chemical Society Petroleum Research Fund for partial support of this research, and RIT Research Computing for technical support. The FDTD software was purchased from www.lumerical.com.

References

[1] J. B. Pendry, A. J. Holden, W. J. Stewart, and I. Youngs, "Extremely low frequency plasmons in metallic mesostructures," *Phys. Rev. Lett.*, vol. 76, no. 25, pp. 4773–4476, Jun. 1996.
[2] R. A. Shelby, D. R. Smith, and S. Schultz, "Experimental verification of a negative index of refraction," *Science*, vol. 292, no. 5514, pp. 77–79, Apr. 2001.
[3] S. Enoch, G. Tayeb, P. Sabouroux, N. Guérin, and P. Vincent, "A metamaterial for directive emission," *Phys. Rev. Lett.*, vol. 89, no. 21, pp. 213902-1–213902-4, Nov. 2002.
[4] N. Garcia, E. V. Ponizovskaya, and J. Q. Xiao, "Zero permittivity materials: Band gaps at the visible," *Appl. Phys. Lett.*, vol. 80, no. 7, pp. 1120-1–1120-3, Dec. 2002.
[5] R. W. Ziolkowski, "Propagation in and scattering from a matched metamaterial having a zero index of refraction," *Phys. Rev. E, Statist., Nonlinear Soft Matter Phys.*, vol. 70, no. 4, pp. 046608-1–046608-12, Oct. 2004.
[6] M. Silveirinha and N. Engheta, "Tunneling of electromagnetic energy through subwavelength channels and bends using ε-near-zero materials," *Phys. Rev. Lett.*, vol. 97, no. 15, pp. 157403-1–157403-4, Oct. 2006.
[7] R. Liu, Q. Cheng, T. Hand, J. J. Mock, T. J. Cui, S. A. Cummer, and D. R. Smith, "Experimental demonstration of electromagnetic tunneling through an epsilon-near-zero metamaterial at microwave frequencies," *Phys. Rev. Lett.*, vol. 100, no. 2, pp. 023903-1–023903-4, Jan. 2008.
[8] M. Silveirinha and N. Engheta, "Design of matched zero-index metamaterials using nonmagnetic inclusions in epsilon-near-zero media," *Phys. Rev. B, Condens. Matter Mater. Phys.*, vol. 75, no. 7, pp. 075119-1–075119-10, Feb. 2007.
[9] A. Alù, M. G. Silveirinha, A. Salandrino, and N. Engheta, "Epsilon-Near-Zero (ENZ) metamaterials and electromagnetic sources: Tailoring the radiation phase pattern," *Phys. Rev. B*, vol. 75, no. 15, pp. 155410-1–155410-13, Apr. 2007.
[10] Z. Lu and W. Zhao, "Nanoscale electro-optic modulators based on graphene-slot waveguides," *J. Opt. Soc. Amer. B*, to be published.
[11] E. D. Palik, *Handbook of Optical Constants of Solids*. Boston, MA: Academic, 1985.
[12] P. Robusto and R. Braunstein, "Optical measurements of the surface plasmon of indium-tin oxide," *Phys. Stat. Sol.*, vol. 119, no. 1, pp. 155–168, May 1990.
[13] H. Brewer and S. Franzen, "Calculation of the electronic and optical properties of indium tin oxide by density functional theory," *Chem. Phys.*, vol. 300, no. 1–3, pp. 285–293, May 2004.
[14] C. Rhodes, S. Franzen, J.-P. Maria, M. Losego, D. N. Leonard, B. Laughlin, G. Duscher, and S. Weibel, "Surface plasmon resonance in conducting metal oxides," *J. Appl. Phys.*, vol. 100, no. 5, pp. 054905-1–054905-4, Sep. 2006.
[15] F. Michelotti, L. Dominici, E. Descrovi, N. Danz, and F. Menchini, "Thickness dependence of surface plasmon polariton dispersion in transparent conducting oxide films at 1.55 μm," *Opt. Lett.*, vol. 34, no. 6, pp. 839–841, Mar. 2009.
[16] P. R. West, S. Ishii, G. V. Naik, N. K. Emani, V. M. Shalaev, and A. Boltasseva, "Searching for better plasmonic materials," *Laser Photon. Rev.*, vol. 4, no. 6, pp. 795–808, Nov. 2010.
[17] E. Feigenbaum, K. Diest, and H. A. Atwater, "Unity-order index change in transparent conducting oxides at visible frequencies," *Nano. Lett.*, vol. 10, no. 6, pp. 2111–2116, Jun. 2010.
[18] M. A. Noginov, L. Gu, J. Livenere, G. Zhu, A. K. Pradhan, R. Mundle, M. Bahoura, Y. A. Barnakov, and V. A. Podolskiy, "Transparent conductive oxides: Plasmonic materials for telecom wavelengths," *Appl. Phys. Lett.*, vol. 99, no. 2, pp. 021101-1–021101-3, Jul. 2011.
[19] G. V. Naik and A. Boltasseva, "A comparative study of semiconductor-based plasmonic metamaterials," *Metamaterials*, vol. 5, no. 1, pp. 1–7, Apr. 2011.
[20] G. V. Naik, J. Kim, and A. Boltasseva, "Oxides and nitrides as alternative plasmonic materials in the optical range," *Opt. Mat. Exp.*, vol. 1, no. 6, pp. 1090–1099, Oct. 2011.
[21] A. Melikyan, N. Lindenmann, S. Walheim, P. M. Leufke, S. Ulrich, J. Ye, P. Vincze, H. Hahn, T. H. Schimmel, C. Koos, W. Freude, and J. Leuthold, "Surface plasmon polariton absorption modulator," *Opt. Exp.*, vol. 19, no. 9, pp. 8855–8869, Apr. 2011.
[22] V. E. Babicheva and A. V. Lavrinenko, *Plasmonic Modulator Optimized by Patterning of Active Layer and Tuning Permittivity*, arXiv:1202.6559v1
[23] A. V. Krasavin and A. Zayats, "Nanoscale photonic transistor," presented at the Integrated Photonics Research, Silicon, Nanophotonics, Optical Society America Tech. Dig. (CD), Toronto, ON, Canada, 2011, Paper IWB2.
[24] Q. Xu, V. R. Almeida, and M. Lipson, "Experimental demonstration of guiding and confining light in nanometer-size low-refractive-index material," *Opt. Lett.*, vol. 29, no. 14, pp. 1626–1628, Jul. 2004.
[25] S. Zhu, G. Q. Lo, and D. L. Kwong, "Electro-absorption modulation in horizontal metal-insulator-silicon-insulator-metal nanoplasmonic slot waveguides," *Appl. Phys. Lett.*, vol. 99, no. 15, pp. 151114-1–151114-3, Oct. 2011.
[26] J. Liu, M. Beals, A. Pomerene, S. Bernardis, R. Sun, J. Cheng, L. C. Kimerling, and J. Michel, "Waveguide-integrated, ultralow-energy GeSi electro-absorption modulators," *Nat. Photon.*, vol. 2, no. 7, pp. 433–437, Jul. 2008.